Available online at www.sciencedirect.com
SCIENCE DIRECT®
International Journal of Heat and Mass Transfer 47 (2004) 5765–5780
International Journal of HEAT and MASS TRANSFER
www.elsevier.com/locate/ijhmt

Modeling the radiation of anisotropically scattering media by coupling Mie theory with finite volume method

D.N. Trivic [a,*], T.J. O'Brien [b], C.H. Amon [a]

[a] *Institute for Complex Engineered Systems, College of Engineering, Carnegie Mellon University, Pittsburgh, PA 15213-3890, USA*
[b] *US Department of Energy, National Energy Technology Laboratory, Morgantown, WV 6507-0880, USA*

Received 24 May 2004
Available online 23 September 2004

Abstract

A new mathematical model and code for radiative heat transfer of particulate media with anisotropic scattering for 2-D rectangular enclosure is developed. The model is based on the coupling of (i) finite volume method for the solution of radiative transfer equation with (ii) Mie equations for the evaluation of scattering phase function. It has not been done before to the authors' best knowledge. The predictions were compared against the only found results, published 15 years ago. For those results the S-N discrete ordinates method for the solution of radiative transfer equation and the Legendre polynomials expansions for the evaluation of scattering phase function were used. The agreement between the results is very good. The advantages of new model and code are in their straight forward application to any given particles parameters without the need for previously designed analytical expression for scattering phase function. In addition, that analytical expression, with generated expansion coefficients, is restricted and can be used only for that particular case of particle parameters. The new model was applied to the solid particles of several various coals and of an ash and the series of 2-D predictions are performed. The effects of particle size parameter and of scattering albedo on radiative heat flux and on incident radiation were analyzed. It was found that the model developed is reliable and very accurate and thus suitable for extension towards: (i) 3-D geometries, (ii) mixtures of non-gray gases with particles as well as for (iii) incorporation in computational fluid dynamics codes.

Keywords: Particles radiation; Anisotropic scattering; Mie theory; Finite volume method

1. Introduction

The radiative heat transfer of particles cloud as well as the radiation of combustion gases–particles mixtures play significant role in many areas and devices. Some of them are pulverized-coal furnaces, cement kilns, fluidized beds and rockets with aluminized solid propellants. In addition, in various combustion chambers, the combustion producing luminous flames contains not only combustion gases but also soot. The particles emit, absorb and scatter radiant energy where the scattering is mainly anisotropic. The mathematical modeling of these phenomena is very important.

There have been many efforts towards the solution of multi-dimensional radiative heat transfer within

* Corresponding author. Address: Nuclear Institute "Vinca", Department of Thermal Engineering and Energy Research, P.O. Box 522, 11001 Belgrade, Serbia and Montenegro. Tel.: +381 11 244 0871x631; fax: +381 11 245 3670.
E-mail address: trivic@vin.bg.ac.yu (D.N. Trivic).

0017-9310/$ - see front matter © 2004 Elsevier Ltd. All rights reserved.
doi:10.1016/j.ijheatmasstransfer.2004.07.035

Nomenclature

a	coefficients of discretization equations
A	area of control volume faces
a_n	Mie scattering coefficient
b	source term in discretization equations
b_n	Mie scattering coefficient
C_j	expansion coefficient of phase function
D^l_{cx}, D^l_{cy}	direction cosines integrated over solid angle control volume $\Delta\Omega$
E	emissive power
$\hat{e}_x, \hat{e}_y, \hat{e}_z$	unit vectors in x, y, and z directions
G	average incident radiation
i	$\sqrt{-1}$
i_1	non-dimensional polarized intensity
i_2	non-dimensional polarized intensity
I	intensity
I_B	blackbody intensity from an opaque wall
I_b	blackbody intensity from a medium
I_w	intensity at opaque diffuse wall
$j_n(z)$	spherical Bessel function of the first kind
k	absorptive index (imaginary part of the complex index of refraction)
L	number of sub-control angles
m	complex index of refraction
$\hat{n}$	unit outward normal vector
n	refractive index (real part of the complex index of refraction)
n	index in infinite series
P_n	Legendre polinomial
q	heat flux
q_w	wall heat flux
Q_{ext}	extinction efficiency factor
Q_{sca}	scattering efficiency factor
Q_{abs}	absorption efficiency factor
r	particle radius
$\vec{r}$	position vector
Re	real part of a complex number
s	distance traveled by a beam
$\hat{s}$	angular direction
S	source function
S_1	complex amplitude function
S_2	complex amplitude function
x, y, z	Cartesian coordinate directions
x	particle size parameter
$y_n(z)$	spherical Bessel function of the second kind

Greek symbols

β	extinction coefficient
γ	scattering angle, same as ψ
$\Delta x, \Delta y$	control volume dimensions in x and y directions
ΔV	volume of control volume
$\Delta\Omega$	solid angle control angle
ε	wall emissivity
κ	absorption coefficient
κ_p	absorption coefficient of particles cloud
λ	the wavelength of incident radiation
μ	direction cosine in the x-direction, $\cos\theta$
ρ	wall reflectivity
θ	polar angle measured from $\hat{e}_z$
σ	scattering coefficient or Stefan Boltzmann constant
ϕ	azimuthal (planar) angle measured from $\hat{e}_x$
Φ	scattering phase function
$\Phi(\gamma)$	scattering phase function for γ argument
$\overline{\Phi}^{l'l}$	normalized scattering phase function, or average scattering phase function, or average energy scattered from solid control angle defined by direction l' to solid control angle defined by direction l
ψ	scattering angle, same as γ
$\psi_n(z)$	Ricatti–Bessel function
$\xi_n(x)$	Ricatti–Hankel function
π_n	direction-dependent (or angular) function
τ_n	direction-dependent (or angular) function

Superscripts

*	non-dimensional variables
+	positive direction
−	negative direction
′	incident direction
l, l'	angular directions

Subscripts

b	blackbody
E, W, N, S	east, west, north and south neighbors of control volume P
P	control volume P
p	related to particles
x, y, z	coordinate directions
w	wall
S	sub-control angle

Abbreviations

ADF	absorption distribution function
BC	boundary condition
CFD	computational fluid dynamics
DOM	discrete ordinate method
DTM	discrete transfer method
FVM	finite volume method
LBL	line-by-line (model)
RTE	radiative transfer equation
SLW	spectral line-based weighted sum of gray gases (model)
SNB	statistical narrow band (model)
TIF	total interchange factors
2-D	two-dimensional
3-D	three-dimensional
WSGGM	weighted sum of gray gases model

particulate media. Two-dimensional radiation was considered by Fiveland [1] where RTE was solved by S-N discrete ordinate method (DOM), but only the problems with isotropic scattering were analyzed. Finite elements were used by Thynell and Ozisik [2] for the analysis of radiation transfer in isotropically scattering rectangular geometries. The P-3 spherical harmonics method for radiative transfer in scattering media in 2-D rectangular geometry was used by Ratzel and Howell [3]. Menguc and Viskanta [4] used P-3 results for radiative transfer in inhomogeneous, anisotropically scattering media in 3-D rectangular enclosures. The integral equation for radiative transfer in a two-dimensional rectangular geometry was solved by removing singularity by Crosbie and Schrenker [5]. In all these 5 multi-dimensional cases only the problems with isotropic or with simple anisotropic scattering media were considered.

Trivic [6] has developed a three-dimensional mathematical model for predicting turbulent flow with combustion and radiative heat transfer within a furnace. The model consists of two sections: (1) transport equations that are non-linear partial differential equations solved by a finite difference scheme, and (2) the radiative heat transfer that was analyzed by the zone method. The link between these two sections is a source–sink term in the energy equation. The radiative properties of combustion gases were represented by two different models: (1) Hottel and Sarofim's model and, (2) Steward's model. The Monte Carlo method was used to evaluate total radiative interchange in the system between zones. The Mie equations were used for the determination of the radiative properties of particles suspended in the combustion gases. The mathematical model was validated against experimental data collected on two large furnaces: (1) A tangentially pulverized-coal-fired boiler of 220 MW; (2) an oil-fired boiler of 345 MW, with symmetrically positioned burners at the front and rear wall. The tests and calculations were performed for several loads for both boilers. The measured and predicted gas temperature and heat flux distributions within the boilers were compared. The results gave reasonable agreement between measurements and values predicted by the model. A series of calculations with varying gas radiative property models, loads, types of fuel, excess air, burner tilt angles and several particle parameters were performed [27]. The effects of these variables on the gas temperature and heat flux distributions within the furnace were studied.

Steward and Trivic studied the radiation of the mixtures of non-gray gas and particles in a pulverized-coal-fired boiler [7]. A mathematical model based on the fundamental equations of motions and energy transfer, and on the zone method for determining radiative heat transfer, was developed for an operating 220 MW pulverized-coal-fired boiler. The scattering phase function for anisotropically scattering was evaluated by Mie Theory. The model is capable of predicting velocity, temperature and heat flux distributions for the three-dimensional combustion chamber. In these models and codes [6,7] the Hottel and Cohen's zone method of analysis for energy balance coupled with the Monte Carlo method for the evaluation of total interchange factors (TIF) was a kind of solution of radiative transfer equation in that time. The Steward and Kocaefe's gas radiative properties model was used. The calculated heat fluxes at the wall have been compared with experimental measurements taken on the boiler for three sets of operating conditions, and they indicated that confidence can be placed in the results.

The comparisons and evaluations of the predictions obtained by those concepts [6,7] with the results of others related to particles radiation with anisotropically scattering, are difficult because the codes [6,7] did not deal with particles radiation only. Those 3-D codes link fluid flow, turbulence model, combustion pattern, heat transfer by convection, conduction and radiation, anisotropic particles scattering and gas radiative properties models. Thus it was very difficult here to carry out the analysis of the role played only by the particles radiation with anisotropically scattering. Besides that, considering the anisotropically scattering of ash particles, the Steward and Trivic's [7] main conclusion was the following. If the particle size of the ash is assumed to be that of mean particle size of the pulverized coal that is fired to the boiler (50 μm), the model indicates that the radiative heat transferred by the particles is negligible. If the ash particles are assumed to be one-tenth this size (5 μm) the model indicates that the radiative heat transfer is increased more than 20%. The model also indicates that for the 5 μm particles the radiative transfer within combustion chamber is significantly affected by the complex refractive index of the ash particles.

The radiative heat transfer in 2-D rectangular geometries was modeled by using S-N discrete ordinates method for solution of radiative transfer equation [8]. The medium in enclosures was gray and it absorbs, emits and anisotropically scatters radiant energy. The anisotropic scattering phase function was evaluated by Legendre polynomials expansions. In that study the radiative intensity field, average incident radiation and the radiative heat flux were predicted. Also the effect of: anisotropy of the scattering phase functions, the aspect ratio, the optical thickness, the scattering albedo and the boundary reflectivity on the radiative transfer were thoroughly examined. The two-dimensional anisotropic scattering cases evaluated there were presented then without comparison since there were no published results for those cases in that time.

An extension of WSGGM to a mixture of non-gray gas and gray particles was presented by Yu et al. [9]. The discrete ordinates method (DOM) was used for the solution of radiative transfer equation which was

coupled with WSGGM. The relation between the weighting factors used in the WSGGM for a mixture of non-gray gas and gray particles with scattering, when the thermal non-equilibrium exist, i.e. the gas and particles temperature are different, has been discussed. This model was applied to two cases. First case was a one-dimensional isothermal mixture of non-gray gas (CO_2, H_2O and transparent inert gas) and soot particles. The Smith et al. WSGGM [10] was used as the gas radiative properties model for the mixture of CO_2, H_2O and transparent inert gas. The algebraic expression based on Rayleigh small particles limit [11], was used for the evaluation of soot absorption coefficient. Second calculation case consisted of a pure scattering medium in a cylindrically symmetric geometry and was used to examine the effect of anisotropy on radiative heat flux. The scattering phase function was presented by the approximation of a finite series of Legendre polynomials.

An efficient method for modeling radiative transfer in multi-component gas mixture with soot was presented by Solovjev and Webb [12]. The method is based on the spectral line weighted sum of gray gases (SLW) model. The gas mixture was considered as a single gas whose absorption distribution function (ADF) was evaluated through the distribution functions of the individual components in the mixture. The soot was taken as another gas in the mixture. The verification of the method was carried out by the comparison with line-by-line (LBL) solution for radiative transfer equation for mixtures of water vapor, carbon dioxide and carbon monoxide with various volume fractions of soot. Their predictions were compared as well with previously published results calculated by statistical narrow band (SNB) model and by WSGGM [13]. The predictions were done for one-dimensional geometry and related to particles material only for soot particles. The calculation of soot absorption coefficient was done by using the Rayleigh small particles limit [11]. In that expression the absorption coefficient is an algebraic relation that depends on real and imaginary part of the complex index of refraction, soot volume fraction and medium temperature.

In the present study a new approach for modeling particles radiation with anisotropic scattering is presented. It is based on the direct coupling of finite volume method (FVM) for the solution of radiative transfer equation (RTE) with general Mie Theory for the rigorous calculation of scattering phase function. The link is through the evaluation of average scattering phase function which plays role within the source term of discretized radiative transfer equation. It was never done before to the authors' best knowledge. The predictions obtained by this methodology were compared with only available results. Those results were calculated by S-N discrete ordinate method with Legendre polynomials expansions for the calculation of scattering phase function and are presented in Kim and Lee's paper [8]. The coefficients of polynomials are tabulated only for some particles size parameters and it brings the limitation in that method [8]. Even the predictions by Kim and Lee [8] and in this study were obtained by various methods they are very close to each other and almost identical.

The advantage of the approach presented in this study is that it can be used directly for the radiation of any particles, once the particles parameters as complex index of refraction, particle mean diameter and the wavelength of incident radiation are known. Here there is no need for previously generated expansion coefficients for the approximated scattering phase functions used only for some particular case.

This method is a step ahead towards 3-D particles radiation with anisotropic scattering, where hardly can be found any benchmark cases. Also once this methodology is validated for 2-D, it can be used as a "building block" or as a "module" for more complex cases as 3-D radiation of non-gray gases–particles mixtures.

2. Mathematical formulations

2.1. Radiative transfer equation for a particles cloud

The particles cloud in this study is considered as a gray medium. The equation for radiative heat transfer for a gray medium can be found in many references, Ozisik [14], Siegel and Howell [15] and Modest [16], as

$$\frac{\mathrm{d}I(\vec{r},\hat{s})}{\mathrm{d}s} = -\beta(\vec{r})I(\vec{r},\hat{s}) + S(\vec{r},\hat{s}) \tag{1}$$

The equation simply indicates that the change of intensity along a path, or the energy accumulation, is equal to the difference between the energy gained and energy lost. The term $-\beta(\vec{r})I(\vec{r},\hat{s})$ represents attenuation and $S(\vec{r},\hat{s})$ accounts for augmentation.

The extinction coefficient β, is given as

$$\beta(\vec{r}) = \kappa(\vec{r}) + \sigma(\vec{r}) \tag{2}$$

where $\kappa(\vec{r})$ represents the absorption of radiant energy and $\sigma(\vec{r})$ accounts for the out-scattering of radiant energy.

The energy source function, $S(\vec{r},\hat{s})$, is given as

$$S(\vec{r},\hat{s}) = \kappa(\vec{r})I_{\mathrm{b}}(\vec{r}) + \frac{\sigma(\vec{r})}{4\pi}\int_{4\pi} I(\vec{r},\hat{s}')\Phi(\hat{s}',\hat{s})\mathrm{d}\Omega' \tag{3}$$

The first term of the right hand side of this expression, $\kappa(\vec{r})I_{\mathrm{b}}(\vec{r})$, accounts for gas emission while the second term represents the accumulation of radiant energy due to in-scattering from all other directions in the domain.

Radiant intensity I depends on spatial position $\vec{r}$ and angular direction $\hat{s}$. For 2-D rectangular enclosure, I depends on four spatial variables, $I(x,y,\theta,\phi)$. Here x,y

are the Cartesian coordinates of the position vector, $\vec{r}$, and θ, ϕ are the polar and planar angles, respectively, that define the intensity direction $\hat{s}(\theta,\phi)$.

The scattering phase function, $\Phi(\hat{s}',\hat{s})$, is equal to unity for isotropic scattering and has various values in various directions, $(\hat{s}',\hat{s})$, for anisotropic scattering.

2.2. Discretized form of radiative transfer equation

Detailed procedure of discretization of radiative transfer equation and of source function is presented in several sources as [17–19]. Therefore this will not be derived and discussed here again. Only final discretized equations needed for the explanation of the link with Mie Theory will be considered and used herewith. Also the radiative heat transfer relations as the incident radiation coming from all directions (i.e., integrated over 4π radians), $G(\vec{r})$, the radiative heat flux in the direction of the unit vector $\hat{i}$ expressed as $q_i(\vec{r})$ and the divergence of the radiative heat flux, designated by $\nabla \bullet q$, used in this work, are presented in details in sources [17,19,20] and they will not be discussed here once again.

By integrating Eq. (1) over control angle and control volume and after that by applying the divergence theorem on its left hand side, Eq. (1) is transformed towards discretization. In finite volume method, the magnitude of the radiative intensity is taken constant over the control angle and control volume. Under these assumptions, for four control volume faces, i.e. for 2-D geometry, Eq. (1) can be written in a simple way as

$$\sum_{i=1}^{4} I_i^l A_i \int_{\Delta\Omega_l} (\hat{s}^l \bullet \hat{n}_i)\,\mathrm{d}\Omega = \int_{\Delta\Omega^l} \int_{\Delta V} (-\beta I^l + S^l)\mathrm{d}V\,\mathrm{d}\Omega \tag{4}$$

where source function written in discretization form is

$$S^l = \kappa I_\mathrm{b} + \frac{\sigma}{4\pi} \sum_{l'=1}^{L} I^{l'} \overline{\Phi}^{l'l} \Delta\Omega^{l'} \tag{5}$$

In Eq. (5), the quantity $\overline{\Phi}^{l'l}$ is the average scattering phase function from control angle l' (that is incident angle) to control angle l (that is scattering angle).

The areas and the volume elements are considered by taking a unit depth in the z-direction. The areas, or four control volume faces, A_E, A_W, A_N and A_S are defined as

$$A_\mathrm{E} = A_\mathrm{W} = \Delta y \cdot 1 \quad A_\mathrm{N} = A_\mathrm{S} = \Delta x \cdot 1 \tag{6}$$

The volume of control volume is denoted as

$$\Delta V_P = \Delta x \Delta y \cdot 1 \tag{7}$$

The areas A_E and A_W are equal for Cartesian coordinates, but the different symbols are used for the sake of generality.

To relate the intensity at the boundaries of control volumes to the nodal intensities, spatial differencing schemes are needed. One of the available schemes is the step scheme, which sets the downstream boundary intensities equal to the upstream nodal intensities. The step scheme was used within this study.

A more compact form of discretization equation suitable for control volume pointing in all directions (and for various marching procedure following directions cosine) is written as

$$a_P^l I_P^l = a_\mathrm{W}^l I_\mathrm{W}^l + a_\mathrm{E}^l I_\mathrm{E}^l + a_\mathrm{S}^l I_\mathrm{S}^l + a_\mathrm{N}^l I_\mathrm{N}^l + b^l \tag{8}$$

Eq. (8) is used to calculate the new values of radiant intensities, and they are calculated as follows:

$$I_P^l = \frac{a_\mathrm{W}^l I_\mathrm{W}^l + a_\mathrm{E}^l I_\mathrm{E}^l + a_\mathrm{S}^l I_\mathrm{S}^l + a_\mathrm{N}^l I_\mathrm{N}^l + b^l}{a_P^l} \tag{9}$$

Detailed derivation and presentation of the other variables related to the discretization is given in [17,19,20] and it will not be discussed here again.

2.3. Discretized boundary conditions

The boundary condition for an opaque diffuse surface given in the form of the boundary intensity is

$$I(\vec{r},\hat{s}) = \varepsilon(\vec{r}) I_\mathrm{b}(\vec{r}) + \frac{\rho(\vec{r})}{\pi} \int_{\hat{s}' \bullet n < 0} I(\vec{r},\hat{s}')|\hat{s}' \bullet \vec{n}|\,\mathrm{d}\Omega' \tag{10}$$

There are two expressions on the right hand side of equation (4). The first one is the emission due to the surface temperature where I_b is the so-called black body radiation. The second term is the reflection of the incoming intensities. The radiation energy leaving an opaque diffusion surface is just the sum of these two effects.

The discretized form of Eq. (10) is as follows:

$$I_\mathrm{w} = \varepsilon_\mathrm{w} I_\mathrm{B} + \frac{\rho_\mathrm{w}}{\pi} \sum_{D_{cx}^{l'}} I_\mathrm{w}^{l'} D_{cx}^{l'} \tag{11}$$

This type of boundary condition, the so-called temperature boundary condition, was used for the problems analyzed in this work within the computer codes developed here. When the heat flux at the wall is prescribed, the intensity leaving that diffuse, opaque wall is given in discretized form as

$$I_\mathrm{w} = \frac{q}{\pi} + \frac{1}{\pi} \sum_{D_{cx}^{l'}} I_\mathrm{w}^{l'} D_{cx}^{l'} \tag{12}$$

There are the other types of boundary conditions as Symmetry Conditions, Periodic Conditions etc, and their detailed description as well as the explanation of the variables can be found in Chai's Ph.D. Thesis [17] and in [18]. If it is needed, the discretized form of those boundary conditions can be easily and quickly incorporated in the codes developed here.

2.4. The link of control volume method with Mie theory

The basic equations and functions of Mie Theory are presented in Appendix A. There are two forms of the normalized scattering phase function also called average scattering phase function, $\overline{\Phi}^{l'l}$, to be used in Eq. (5). They are: (i) the form when analytical expression for scattering phase function exists (various approximations as a finite series of Legendre polynomials etc.) and (ii) the form when analytical expression for scattering phase function does not exist and scattering phase function will be evaluated through complex procedure related to Mie equations.

For the first form, when the analytical expression for scattering phase function exists, the average scattering phase function can be calculated then as

$$\overline{\Phi}^{l'l} = \frac{\int_{\mathrm{d}\Omega^{l'}} \Phi(\hat{s}', \hat{s})\mathrm{d}\Omega'}{\Delta\Omega^{l'}} \tag{13}$$

For the second form, when the analytical expression for scattering phase function does not exist, the average scattering phase function is calculated as

$$\overline{\Phi}^{l'l} = \frac{\int_{\Delta\Omega^{l}} \int_{\mathrm{d}\Omega^{l'}} \Phi(\hat{s}', \hat{s})\mathrm{d}\Omega'\,\mathrm{d}\Omega}{\Delta\Omega^{l}\Delta\Omega^{l'}} = \frac{\sum_{l_\mathrm{S}=1}^{L_\mathrm{S}} \sum_{l'_\mathrm{S}=1}^{L'_\mathrm{S}} \Phi^{l'_\mathrm{S} l_\mathrm{S}} \Delta\Omega^{l'_\mathrm{S}} \Delta\Omega^{l_\mathrm{S}}}{\Delta\Omega^{l}\Delta\Omega^{l'}} \tag{14}$$

The analytical expressions for the scattering phase functions for various particle materials considered within this study do not exist. Thus the Eq. (14) is used in this work. More details on the derivation of the Eq. (14) are given in Ref. [19].

The average scattering phase function, $\overline{\Phi}^{l'l}$ used in Eq. (5) within calculation of source function, depends inter alia on the discrete values of scattering phase function, i.e. on $\Phi^{l'_\mathrm{S} l_\mathrm{S}}$ values. The $\overline{\Phi}^{l'l}$ is calculated by using Eq. (14). The values of $\Phi^{l'_\mathrm{S} l_\mathrm{S}}$ are in turn evaluated from Mie equations using the following expression:

$$\Phi^{l'_\mathrm{S} l_\mathrm{S}} = \Phi(\gamma) = 2\frac{i_1 + i_2}{x^2 Q_{\mathrm{sca}}} \tag{15}$$

Eq. (15) is actually Eq. (A.1) from Appendix A where its derivation and explanation are presented in more details. That is the link of finite volume method with Mie Theory.

It should be mentioned that in Eq. (14) each of the solid angle sub-control angle, i.e. $\Delta\Omega^{l'_\mathrm{S}}$ and $\Delta\Omega^{l_\mathrm{S}}$, is defined with two, polar and asimuthal, angles and that the summation over each of them should be performed. Therefore, within Eq. (14), double summation sign in denominator will be transformed into four summation signs and those have been introduced in the code during the computer program writing.

All values of scattering angles which are defined by the sub-control angles $\Delta\Omega^{l'_\mathrm{S}}$ and $\Delta\Omega^{l_\mathrm{S}}$, i.e. by the incident and scattering directions $\widehat{S}'$ and $\widehat{S}$, respectively, must be known and then for them as the arguments, the values of scattering phase function can be evaluated. Those scattering angles are evaluated by applying the following expression:

$$\cos\psi = \mu\mu' + (1-\mu^2)^{1/2}(1-\mu'^2)^{1/2}\cos(\phi' - \phi) \tag{16}$$

After that, for the scattering angle ψ, somewhere designated as γ, evaluated in this way, the scattering phase function $\Phi^{l'_\mathrm{S} l_\mathrm{S}}$ for given particles parameters as particle diameter D_p and complex index of refraction m and for known wavelength of incident radiation λ (or for given particle size parameter x) is calculated by using Eq. (15). Also it could be written that $\Phi^{l'_\mathrm{S} l_\mathrm{S}} = \Phi(\gamma, D_\mathrm{p}, m, \lambda)$.

Therefore the value $\Phi^{l'_\mathrm{S} l_\mathrm{S}}$ that is the value of scattering phase function for the scattering from a discrete incident direction $\widehat{S}'$ into discrete scattering direction $\widehat{S}$ must be known before the Eq. (14) can be applied.

For the evaluation of average scattering phase function, Kim and Lee [8] and Chai et al. [18] used Eq. (13), i.e. they used the analytical expression for scattering phase function that was the approximation by a finite series of Lagendre polynomials. In this work, not having and using analytical expressions, the evaluation of average scattering phase function was carried out by applying Eq. (14) and by using Mie equations.

It should be mentioned that to the authors' best knowledge, inter alia, the implementation and validation of Eq. (14) for the radiation of anisotropically scattering media is never reported in literature so far.

3. Numerical features

The new original computer code that solves radiative transfer equations in 2-D Cartesian coordinates based on finite volume method and linked with Mie equations is developed. The spatial differencing scheme used in this work to relate the boundary intensities to nodal intensities is step scheme. This scheme sets the downstream boundary intensities equal to the upstream nodal intensities.

The process of intensity calculation is repeated for all specified intensity directions and a solution is considered converged when it satisfies the following criterion:

$$|I_P^l - I_P^{l^0}|/I_P^l \leqslant 10^6 \tag{17}$$

Here I_P^l is the latest and $I_P^{l^0}$ the previous iteration.

The scheme appeared to be very efficient. The guess of initial intensity field is set to zero. The solution converges relatively fast. For the particular cases of anisotropic scattering in 2-D geometry where the particles cloud is considered as a gray medium, the incident heat

flux to the accuracy of six decimal points is achieved, depending on the case analyzed, within 12 or 13 iterations. But it should be mentioned that, for 2-D geometry, within an iteration, the code has four sweeps, each of which in one of four "quadrant directions".

The square enclosure is subdivided into 25×25 control volumes. The previous analysis for a gray medium [18,20] as well as the results used for comparison [8,18] show that the results are grid independent.

The angular discretization has the number of increments in polar and azimuthal directions 6×24, respectively. The number of increments in polar and azimuthal directions of sub-control angles, within a control angle, is 3×3, respectively. Thus, the total number of solid sub-control angles, within a control angle, is taken $3 \times 3 = 9$ and is the same for both, incident and scattering directions.

The numerical experiments were performed by changing the number of solid angle control angles. The subdivisions as 3×4, 3×5, 4×4, 4×5, 4×6 etc. were carried out and it was found that the increase of sub-control angles did not influence on the accuracy.

The computer program is written in the way that Mie equations, presented in Appendix A, are used straight forward without the previous design of scattering phase function in the form of an analytical expression. That explicit analytical expression is limited and valid only for the case that is designed for.

Related to Mie equations the following numerical features should be mentioned. For the designation "infinite refractive index" the value of 10^8 is taken. The larger values did not affect the results. Also for the definition of "very small particles" the value of $D_p = 0.01\,\mu m$ is taken, because the smaller values, (here is taken $\lambda = \pi$), i.e. for $x < 0.01$, did not influence on the predictions for function B2. The infinite series, as e.g. direction-dependent functions π_n and τ_n as well as the other relations defined as infinite series, were terminated for the value $n = 1.2x + 9$ that was proposed by Deirmendjian et al. [24].

4. Calculation cases performed

The geometry considered is a square enclosure with side dimension 1.0 presented in Fig. 1. All the walls of the enclosure are black, i.e. for all of them $\varepsilon = 1$ and $\rho = 0$.

The wall designated as "wall 3" is taken as a hot having constant emissive power $E_{b3} = 1.0$. The other walls are kept cold and their emissive powers are $E_{b1} = E_{b2} = E_{b4} = 0$. The enclosure contains pure scattering medium, i.e. for that medium the scattering albedo is equal to unity ($\omega = 1$), the absorption coefficient of medium (particles cloud) is equal to zero ($\kappa_p = 0$) and scattering coefficient is taken as unity ($\sigma = 1$).

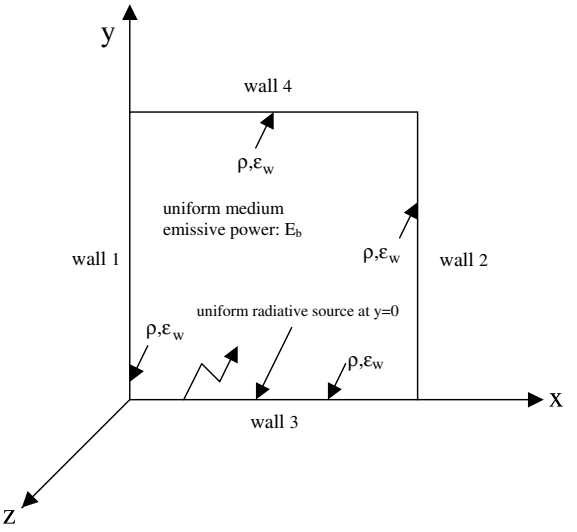

Fig. 1. System geometry.

Two sets of predictions were carried out within this study: (i) the series of predictions to be compared with the results published by Kim and Lee [8] and (ii) a set of results for a group of different coals and for an ash. Detailed description of the problem (i) is given in Lee and Kim's paper [8].

From the point of view of isotropy and anisotropy, five different cases were considered: one isotropic having the designation ISO and four anisotropic cases having the scattering phase functions designated with F1, F2, B1 and B2 [8]. With capital letters F and B are indicated the scattering phase functions that have the peaks in forward and backward directions, respectively. The data related to particles parameters for the evaluation of scattering phase functions F1, F2, B1 and B2 are presented in Table 1.

The dimensionless quantities to be calculated are the average incident radiation $G_y^* = G/4E$ and net radiative heat flux in y-direction $Q_y^* = Q_y/E$. The y-direction is emphasized here because the anisotropy of scattering phase functions plays important role in the radiative heat transfer when the boundary conditions are not symmetric. This is the case here in y-direction because the emissive power of "wall 3" is equal to unity and the emissive power of "wall 4" is equal to zero. For the system with symmetric boundary conditions the effects of anisotropy are cancelled out to give isotropic results, regardless of anisotropy of the scattering phase functions involved. The net radiative heat flux in y-direction $Q_y^* = Q_y/E$ is evaluated as the difference of radiative heat flux in positive y-direction $Q_y^{+*} = Q_y^+/E$ and of radiative heat flux in negative y-direction $Q_y^{-*} = Q_y^-/E$.

With the methodology developed here and with the computer code written within this study for finite

Table 1
Data for evaluation of scattering phase functions F1, F2, B1 and B2 by Mie equations

Scattering phase function designation	Particle size parameter $x = D_p\pi/\lambda$	Real part of complex index of refraction (refractive index) n	Imaginary part of complex index of refraction (absorptive index) k
F1	5	1.33	0
F2	2	1.33	0
B1	1	Very large, taken 10^8	0
B2	D_p very small, taken $x = 0.01$	Very large, taken 10^8	0

Table 2
Data of complex refractive index for different colas and an ash in near infrared region taken from [16] for the evaluation of scattering phase functions

Coal or ash	Particle size parameter $x = D_p\pi/\lambda$	Real part of complex index of refraction (refractive index) n	Imaginary part of complex index of refraction (absorptive index) k
Carbon	1	2.20	1.120
Anthracite	1	2.05	0.540
Bituminous	1	1.85	0.220
Lignite	1	1.70	0.066
Ash	1	1.50	0.020

volume method coupled with Mie equations, the new calculation cases are carried out. In this cases the geometry, the input parameters of the system ($\rho = 0$, $\omega = 1$, $\sigma = 1$, $\kappa_p = 0$) and all the boundary conditions ($\rho, \varepsilon, E_{wb}$, E_B) are the same as in previous case and in [8]. Everything is the same except particles materials that are now: carbon, anthracite, bituminous, lignite and an ash. The data for evaluation of scattering phase functions for coals and ash considered related to near infrared region are taken from [16, Chapter 10], and is presented in Table 2. Instead of artificial media with anisotropic scattering, now the real engineering fuels are considered. The particle size parameters for all materials are taken as unity. It should be mentioned that here again, as in previous cases, particles concentrations and particles diameters are implicitly set or defined through chosen σ, κ_p, x and ω, and they are not explicitly expressed here.

5. Results and discussion

For the sake of comparison of the predictions obtained by new model, and to validate the new code before its application to new cases and before the model development could be proceeded towards 3-D geometry, the only available results, that are the calculation cases performed by Kim and Lee [8], were considered and taken as the benchmark. It should be mentioned that some of the Kim and Lee's results [8] were reproduced by Chai et al. [18]. They used finite volume method for the solution of radiative transfer equation but for the evaluation of scattering phase function they also took the approximation by a finite series of Legendre polynomials.

As a test, the 37 values of scattering phase function (i.e. for the whole region of scattering angles between 0° and 180°, with increments of 5°) for each of the scattering phase functions F1, F2, B1 and B2, were calculated by the new model and code. These values were compared with the scattering phase function curves presented in [8]. The new and old curves could not be distinguished because the values are very close to each other and almost identical. The other predictions for functions F1, F2, B1 and B2 calculated by the code written within this study are also very close to the results given in [8] and they are presented here. Therefore the comparisons can not be presented in graphical form and the predictions are given in tabular form.

In Tables 3 and 4 are presented the results generated by Kim and Lee [8] where RTE was solved by S-N discrete ordinates method and scattering phase functions were evaluated by the approximation of a finite series of Legendre polynomials.

In Tables 5 and 6 are shown the predictions calculated in this study where RTE is solved by finite volume method and scattering phase functions are calculated by Mie equations and then coupled with FVM.

The non-dimensional net radiative heat flux Q_y^* in y-direction along the centerline ($x = 0.5$) for different phase functions (for parameters $\rho = 0$, $\omega = 1$, $\sigma = 1$, $\kappa_p = 0$, square enclosure 1×1) predicted by Kim and Lee [8] and by this study are presented in Tables 3 and 5, respectively. The non-dimensional average incident

Table 3
Non-dimensional net radiative heat flux Q_y^* in y-direction along the centerline ($x = 0.5$) for isotropic and anisotropic scattering for four different phase functions predicted by Kim and Lee [8]: ($\rho = 0$, $\omega = 1$, $\sigma = 1$, $\kappa_p = 0$, square enclosure 1×1)

$y(m)$	ISO	F1	F2	B1	B2
0.020	0.747546	0.945954	0.909987	0.706159	0.665768
0.060	0.728379	0.930752	0.893455	0.686828	0.646392
0.100	0.706271	0.911806	0.873262	0.664805	0.624567
0.140	0.683518	0.892072	0.851966	0.642318	0.602443
0.180	0.660155	0.871542	0.829618	0.619373	0.579992
0.220	0.635295	0.848916	0.805209	0.595081	0.556332
0.260	0.608619	0.823535	0.778325	0.569125	0.531152
0.300	0.580580	0.795751	0.749412	0.541947	0.504883
0.340	0.551957	0.766425	0.719313	0.514303	0.478258
0.380	0.523486	0.736463	0.688861	0.486905	0.451960
0.420	0.495735	0.706615	0.658723	0.460295	0.426506
0.460	0.469084	0.677425	0.629366	0.434831	0.402230
0.500	0.443748	0.649236	0.601073	0.410712	0.379316
0.540	0.419826	0.622244	0.573995	0.388026	0.357839
0.580	0.397358	0.596557	0.548208	0.366802	0.337817
0.620	0.376352	0.572229	0.523748	0.347042	0.319247
0.660	0.356797	0.549284	0.500628	0.328729	0.302108
0.700	0.338667	0.527717	0.478836	0.311831	0.286362
0.740	0.321920	0.507498	0.458344	0.296300	0.271957
0.780	0.306497	0.488580	0.439109	0.282073	0.258824
0.820	0.292332	0.470905	0.421082	0.269074	0.246886
0.860	0.279361	0.454411	0.404216	0.257232	0.236062
0.900	0.267533	0.439043	0.388476	0.246487	0.226286
0.940	0.256818	0.424754	0.373843	0.236797	0.217509
0.980	0.247184	0.411503	0.360318	0.228112	0.209670

Table 4
Non-dimensional average incident radiation G^* along the centerline ($x = 0.5$) for isotropic and anisotropic scattering for four different phase functions predicted by Kim and Lee [8]: ($\rho = 0$, $\omega = 1$, $\sigma = 1$, $\kappa_p = 0$, square enclosure 1×1)

$y(m)$	ISO	F1	F2	B1	B2
0.020	0.600355	0.518740	0.535868	0.616569	0.632666
0.060	0.556250	0.484921	0.498624	0.570840	0.585263
0.100	0.512708	0.449798	0.461528	0.525645	0.538400
0.140	0.474531	0.419550	0.429650	0.485822	0.496928
0.180	0.441868	0.394810	0.403170	0.451563	0.461070
0.220	0.412683	0.373385	0.379963	0.420857	0.428843
0.260	0.385379	0.353413	0.358333	0.392118	0.398681
0.300	0.359364	0.334146	0.337640	0.364761	0.369998
0.340	0.334617	0.315545	0.317857	0.338761	0.342773
0.380	0.311256	0.297782	0.299127	0.314241	0.317122
0.420	0.289369	0.281022	0.281556	0.291279	0.293117
0.460	0.268964	0.265367	0.265191	0.269885	0.270764
0.500	0.249999	0.250859	0.250021	0.250002	0.249999
0.540	0.232387	0.237473	0.235981	0.231539	0.230725
0.580	0.216013	0.225155	0.222990	0.214376	0.212815
0.620	0.200763	0.213820	0.210952	0.198395	0.196136
0.660	0.186516	0.203371	0.199764	0.183463	0 180560
0.700	0.173155	0.193714	0.189331	0.169461	0.165955
0.740	0.160570	0.184751	0.179558	0.156275	0.152204
0.780	0.148657	0.176397	0.170359	0.143791	0.139191
0.820	0.137300	0.168568	0.161635	0.131900	0.126801
0.860	0.126371	0.161186	0.153281	0.120471	0.114907
0.900	0.115699	0.154161	0.145179	0.109337	0.103343
0.940	0.105067	0.147404	0.137162	0.098291	0.091917
0.980	0.094238	0.140816	0.129025	0.087135	0.080447

Table 5
Non-dimensional net radiative heat flux Q_y^* in y-direction along the centerline ($x = 0.5$) for isotropic and anisotropic scattering for four different phase functions predicted by this study: ($\rho = 0$, $\omega = 1$, $\sigma = 1$, $\kappa_p = 0$, square enclosure 1×1)

$y(m)$	ISO	F1	F2	B1	B2
0.020	0.737175	0.940655	0.901298	0.696537	0.656565
0.060	0.717401	0.922917	0.883463	0.676615	0.636702
0.100	0.694634	0.901454	0.861876	0.653952	0.614333
0.140	0.669764	0.877278	0.837545	0.629392	0.590250
0.180	0.643234	0.850795	0.810945	0.603348	0.564840
0.220	0.615609	0.822573	0.782679	0.576362	0.538621
0.260	0.587549	0.793342	0.753470	0.549069	0.512207
0.300	0.559631	0.763776	0.723971	0.522022	0.486121
0.340	0.532271	0.734379	0.694666	0.495615	0.460736
0.380	0.505746	0.705497	0.665890	0.470104	0.436292
0.420	0.480238	0.677363	0.637869	0.445657	0.412941
0.460	0.455867	0.650139	0.610762	0.422383	0.390780
0.500	0.432710	0.623937	0.584676	0.400347	0.369866
0.540	0.410812	0.598827	0.559680	0.379586	0.350230
0.580	0.390188	0.574846	0.535811	0.360110	0.331874
0.620	0.370835	0.552005	0.513080	0.341908	0.314784
0.660	0.352730	0.530295	0.491480	0.324955	0.298930
0.700	0.335842	0.509688	0.470988	0.309213	0.284272
0.740	0.320130	0.490149	0.451573	0.294641	0.270766
0.780	0.305552	0.471635	0.433198	0.281189	0.258359
0.820	0.292059	0.454098	0.415825	0.268806	0.246997
0.860	0.279603	0.437490	0.399416	0.257439	0.236623
0.900	0.268139	0.421763	0.383938	0.247032	0.227177
0.940	0.257626	0.406877	0.369371	0.237536	0.218602
0.980	0.248033	0.392798	0.355711	0.228905	0.210840

Table 6
Non-dimensional average incident radiation G^* along the centerline ($x = 0.5$) for isotropic and anisotropic scattering for four different phase functions predicted by this study: ($\rho = 0$, $\omega = 1$, $\sigma = 1$, $\kappa_p = 0$, square enclosure 1×1)

$y(m)$	ISO	F1	F2	B1	B2
0.020	0.590398	0.507442	0.527234	0.605738	0.621197
0.060	0.546130	0.472158	0.489494	0.559842	0.573665
0.100	0.505758	0.440141	0.455536	0.517819	0.529995
0.140	0.470171	0.412549	0.426196	0.480619	0.491188
0.180	0.438055	0.388023	0.400071	0.446966	0.456008
0.220	0.408335	0.365416	0.376030	0.415800	0.423408
0.260	0.380588	0.344299	0.353633	0.386699	0.392974
0.300	0.354705	0.324600	0.332782	0.359557	0.364593
0.340	0.330623	0.306302	0.313427	0.334306	0.338196
0.380	0.308242	0.289344	0.295486	0.310843	0.313675
0.420	0.287434	0.273632	0.278847	0.289034	0.290889
0.460	0.268062	0.259059	0.263393	0.268737	0.269693
0.500	0.250000	0.245526	0.249016	0.249819	0.249945
0.540	0.233130	0.232940	0.235615	0.232156	0.231515
0.580	0.217343	0.221221	0.223104	0.215634	0.214282
0.620	0.202538	0.210291	0.211400	0.200143	0.198132
0.660	0.188617	0.200080	0.200425	0.185583	0.182956
0.700	0.175489	0.190521	0.190109	0.171854	0.168650
0.740	0.163064	0.181552	0.180382	0.158861	0.155115
0.780	0.151253	0.173112	0.171175	0.146513	0.142253
0.820	0.139965	0.165143	0.162420	0.134714	0.129968
0.860	0.129099	0.157587	0.154042	0.123365	0.118156
0.900	0.118525	0.150377	0.145943	0.112336	0.106692
0.940	0.108045	0.143422	0.137972	0.101439	0.095394
0.980	0.097355	0.136584	0.129869	0.090400	0.084011

radiation G^* along the centerline ($x = 0.5$) for different phase functions (for parameters $\rho = 0$, $\omega = 1$, $\sigma = 1$, $\kappa_p = 0$, square enclosure 1×1) predicted by Kim and Lee [8] and by this study are presented in Tables 4 and 6, respectively.

Comparing the values for heat flux Q_y^* from Table 5 against the values in Table 3 as well as the values for incident radiation G^* from Table 6 against the values in Table 4, it can be seen that they are very close to each other. The differences between them are very small (maximum couple of percent) and it can be said that the agreement between them is excellent. This agreement is the confirmation that Kim and Lee's results [8], published in 1988, were correct and that, at the same time, the methodology developed in this work based on different numerical techniques is very accurate. Instead of using analytical expression for scattering phase function which is manly, if not always, an approximation defined for the specific case and which needs considerably previous work, the Mie Theory was applied herewith. To the authors' best knowledge it was not done before.

Besides these, the following new predictions are performed and presented herewith.

In Fig. 2(a) the scattering phase functions versus scattering angle for five different particles materials, i.e. for carbon, anthracite, bituminous, lignite and an ash, are presented. In Fig. 2(b) the scattering phase functions versus scattering angle for five different values of particle size parameters are given.

In Fig. 3(a)–(c) are presented the predictions for five different particle materials for conditions $\rho = 0$, $\omega = 1$, $\sigma = 1$, $\kappa_p = 0$, square enclosure 1×1, and for particle size parameter $x = 1$. They are: in Fig. 3(a) non-dimensional net radiative heat flux in y-direction, Q_y^*, along the centerline ($x = 0.5$); in Fig. 3(b) non-dimensional average incident radiation, G^*, along the centerline ($x = 0.5$); and in Fig. 3(c) non-dimensional net radiative heat flux on hot surface (wall 3) in y-direction, Q_y^*, along the x-axis.

In Fig. 2(a) can be seen that, under the defined conditions and for the materials considered, the curves of scattering phase functions have the same shape and the differences between them are very small. In turn the differences between predicted values of net radiative heat flux, Q_y^*, and of average incident radiation, G^*, presented in Fig. 3(a) and (b), respectively, appeared to be insignificant. The particle materials analyzed gave almost the same Q_y^* and G^* curves. Some small differences of net radiative heat flux on hot surface (wall 3) for the same group of materials can be noticed in Fig. 3(c). The differences are largest at the values of x-axis $x = 0.5$ and at this location they vary approximately between 0.81 and 0.83. The anthracite gave the largest and the fly ash the smallest value of net radiative heat flux on hot surface.

In Fig. 4(a)–(c) are presented the predictions for fly ash for five different particle size parameters for conditions $\rho = 0$, $\omega = 1$, $\sigma = 1$, $\kappa_p = 0$, square enclosure 1×1. They are: in Fig. 4(a) non-dimensional net radiative heat flux in y-direction, Q_y^*, along the centerline ($x = 0.5$); in Fig. 4(b) non-dimensional average incident radiation, G^*, along the centerline ($x = 0.5$); and in Fig. 4(c) non-dimensional net radiative heat flux on hot surface (wall 3) in y-direction, Q_y^*, along the x-axis. It can be seen in Fig. 4(a) and (b) that there are no variation of Q_y^* and of G^*, respectively for values of particle size parameters $x > 3.0$. The values of $x = 3.0$ and $x = 5.0$ produce the same Q_y^* and G^* curves. It should be mentioned that the calculations were performed as well for the particle size parameters x less than 0.1, i.e. for $x = 0.05$ and smaller, and the predictions of Q_y^*, G^* and of the net heat flux at hot surface are very close to the predictions found for $x = 0.1$. It appears that for the fly ash and under the conditions considered, all the

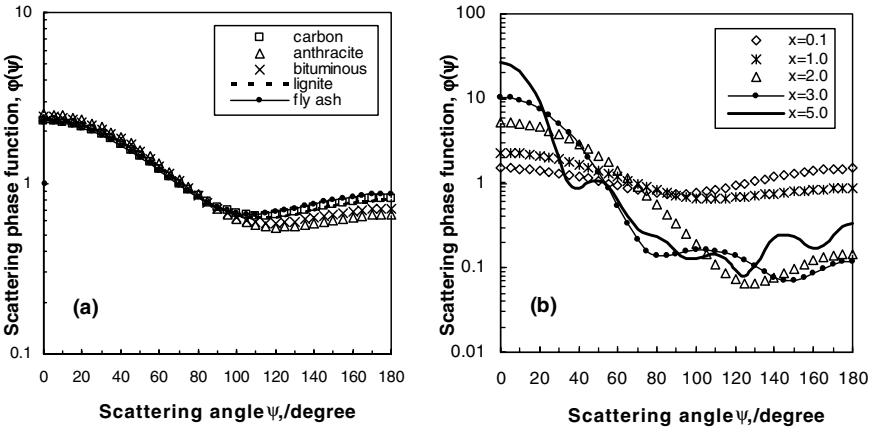

Fig. 2. Scattering phase functions for: (a) different particle materials with particle size parameters $x = 1$; (b) fly ash for different particle size parameters, x.

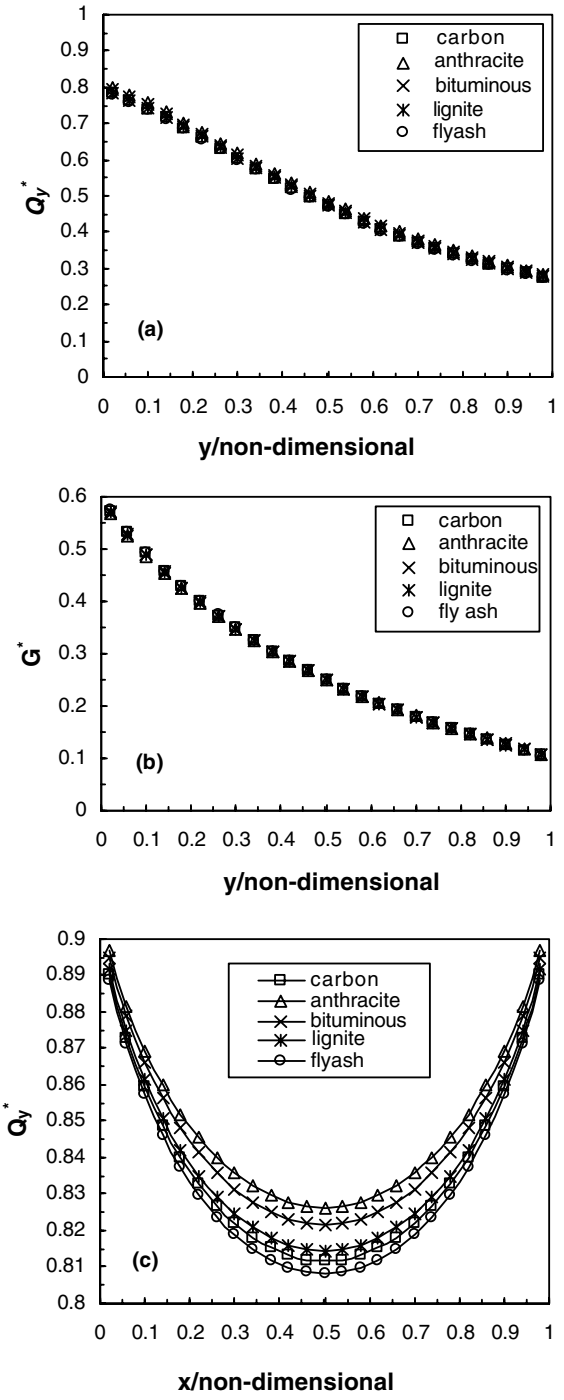

Fig. 3. Predictions for different particle materials ($\rho = 0$, $\omega = 1$, $\sigma = 1$, $\kappa_p = 0$, square enclosure 1×1, particle size parameters $x = 1$): (a) non-dimensional net radiative heat flux in y-direction, Q_y^*, along the centerline ($x = 0.5$); (b) non-dimensional average incident radiation, G^*, along the centerline ($x = 0.5$); (c) non-dimensional net radiative heat flux on hot surface (wall 3) in y-direction, Q_y^*, along the x-axis.

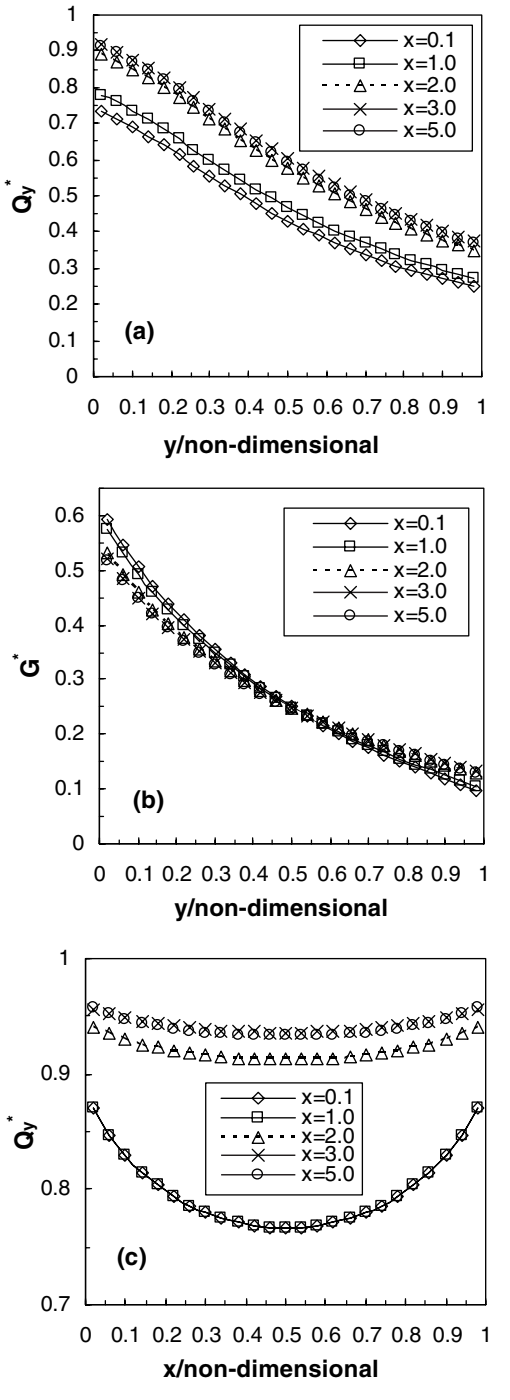

Fig. 4. Predictions for fly ash for different particle size parameters, x ($\rho = 0$, $\omega = 1$, $\sigma = 1$, $\kappa_p = 0$, square enclosure 1×1): (a) non-dimensional net radiative heat flux in y-direction, Q_y^*, along the centerline ($x = 0.5$); (b) non-dimensional average incident radiation, G^*, along the centerline ($x = 0.5$); (c) non-dimensional net radiative heat flux on hot surface (wall 3) in y-direction, Q_y^*, along the x-axis.

variations of Q_y^*, G^* and of the net heat flux on hot surface took place between $x = 0.1$ and $x = 3.0$.

It can be noticed in Fig. 4(a) that the larger value of particle size parameter x produce the larger Q_y^*. Also the smaller is the y-dimensions, (i.e. the closer to the hot surface, wall 3, is a location) the higher is Q_y^*. In Fig. 4(b) can be seen that up to certain value of y-axis (approximately up to $y = 0.5$) the smaller is particle size parameter x, the larger is G^*. From that value of y-axis on, the situation is vice versa, i.e. the larger is x, the larger is G^*. In Fig. 4(c) can be noticed that the larger values of particle size parameter x produce the higher value of net heat flux at hot surface (wall 3). The largest differences of this heat flux are at the values of x-axis $x = 0.5$ and at this location they vary approximately between 0.75 and 0.95.

In Fig. 5(a) and (b) are given the predictions for fly ash for six different values of scattering albedo ω for $\rho = 0$, square enclosure 1×1, and for particle size parameter $x = 1$. They are: in Fig. 5(a) non-dimensional net radiative heat flux in y-direction, Q_y^*, along the centerline ($x = 0.5$) and in Fig. 5(b) non-dimensional average incident radiation, G^*, along the centerline ($x = 0.5$).

It can be noticed in Fig. 5(a) that up to certain value of y-axis (approximately up to $y = 0.15$) the smaller is scattering albedo ω, the larger is Q_y^*. From that value of y-axis on, the situation is vice versa, i.e. the larger is scattering albedo, the higher is the net radiative heat flux in y-direction, Q_y^*, along the centerline. This effect of scattering albedo was noticed, discussed and explained by Kim and Lee [8].

In Fig. 5(b) can be seen that the larger is scattering albedo ω, the higher is the average incident radiation, G^*, along the centerline.

In Fig. 6 are presented the predictions of non-dimensional net radiative heat flux on hot surface (wall 3) in y-direction, Q_y^*, along the x-axis for fly ash for six different values of scattering albedo ω for $\rho = 0$, square enclosure 1×1 and for particle size parameters $x = 1$.

It can be noticed in Fig. 6 that the smaller is scattering albedo ω, the higher is the net radiative heat flux on hot surface (wall 3), Q_y^*. The largest differences of this heat flux are at the values of x-axis $x = 0.5$ and at this location they vary approximately between 0.81 and 1.0.

In general, there are the variations of complex refractive indices m with wavelength. But within this study the particles cloud was considered as a gray medium and the average representative values of m in the near infrared region were taken as they are given by Modest [16].

It should be emphasized that the calculation conditions as $\omega = 1$, $\sigma = 1$, $\kappa_p = 0$ are taken from [8] for the sake of comparison of the predictions calculated in this study with only available results, i.e. for the sake of testing and validating of the model and code developed. The same conditions were used for new sets of predictions related to the group of coals and to the effect of particle size parameter and scattering albedo. Those conditions are arbitrary and artificial. In many cases they do not coincide with real situations in combustion chambers. Within industrial modeling of furnaces, the absorption coefficients κ_p and the scattering coefficients σ of particles cloud are evaluated by using absorption efficiency factor Q_{abs} and scattering efficiency factor Q_{sca}, respectively. These efficiency factors are in turn calculated by Mie Theory as it is presented in Appendix A.

The mathematical model developed in this work is tested and verified against the results available in literature. It appears that this is a reliable numerical structure

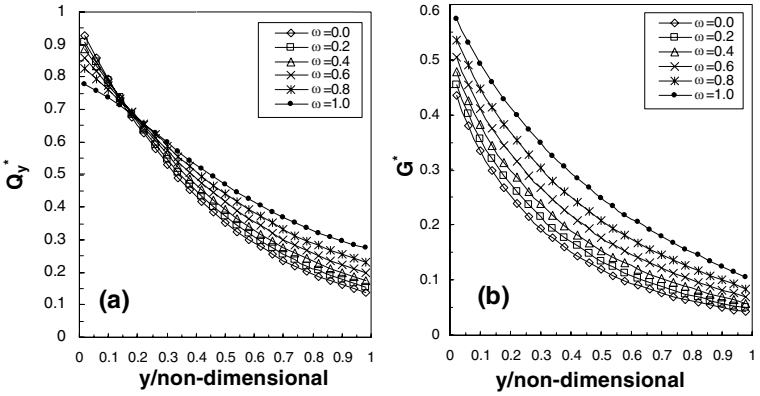

Fig. 5. Predictions for fly ash for different values of scattering albedo ω ($\rho = 0$, square enclosure 1×1, particle size parameters $x = 1$): (a) non-dimensional net radiative heat flux in y-direction, Q_y^*, along the centerline ($x = 0.5$); (b) non-dimensional average incident radiation, G^*, along the centerline ($x = 0.5$).

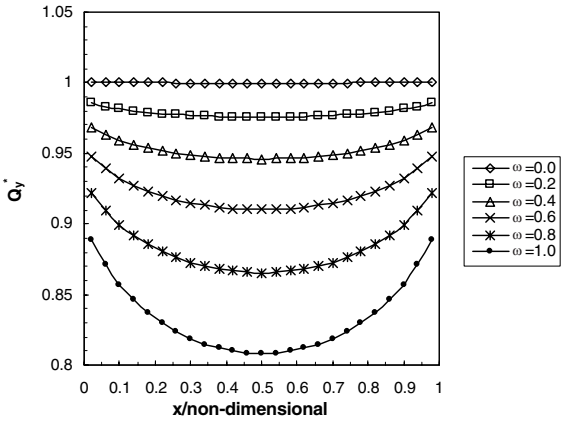

Fig. 6. Predictions of non-dimensional net radiative heat flux on hot surface (wall 3) in y-direction, Q_y^*, along the x-axis for fly ash for different values of scattering albedo ω ($\rho = 0$, square enclosure 1×1, particle size parameters $x = 1$).

that could be built in more realistic physical situations in combustion systems where the anisotropic scattering processes are much more complex. These systems are the following: (i) the different kinds of particles as burning coal (i.e. char), soot and fly ash exist simultaneously and all of them have various particles diameters and different material properties as complex refractive index and density; (ii) the mixtures of particles and of non-gray gases take place in combustion chamber and (iii) the particulate medium is not gray because the complex refractive index varies within wavelength region, i.e. the anisotropic scattering occurs not only for one averaged value of wavelength λ but within whole relevant region of wavelengths.

6. Conclusions

1. A new mathematical model and computer code for particles radiation with anisotropic scattering in 2-D rectangular geometry based on coupling of FVM with Mie Theory is developed. The physical and mathematical concepts of the model are discussed in details. The series of predictions were performed for pure scattering media. The predictions were compared against the only results found in literature where the different numerical techniques were used for the solution of RTE and for the evaluation of scattering phase function. The agreements between the predictions calculated in this study with those found in published paper are very good.
2. The new predictions for a group of materials as carbon, anthracite, bituminous, lignite and an ash, which are more realistic and close to the real combustion processes were produced. Also the effects of particle size parameter and of scattering albedo on radiative heat flux and on incident radiation for fly ash were analyzed. For the input data given and for the conditions specified, these predictions present more information on anisotropic scattering of fuels and fly ash considered. In addition, they can be used for comparisons with predictions to be provided by others.
3. Under the conditions considered if the different particle materials have the same shape of scattering phase functions with small differences between them, it will result in the same values of net radiative heat flux and of average incident radiation for all those materials.
4. For the fly ash analyzed, only the values of particle size parameters x in the region $0.1 < x < 3.0$ influence on the net radiative heat flux, Q_y^*, and on the average incident radiation, G^*.
5. Compared to the previous methods, the advantage of introduction of complex Mie equations is that the additional work, previously needed for the design of analytical expressions for scattering phase functions, is avoided. Mie equations are directly applicable to any materials, dimensions and parameters of particles. Besides, that explicit analytical expression is limited and valid only for the case that is designed for. Also, FVM is widely used for solving transport equations within CFD codes nowadays and it makes this code compatible and convenient for coupling with CFD codes.
6. The 2-D version of the model is validated and it appeared that the model and code are reliable and very accurate. Therefore the methodology can be extended towards: (i) 3-D geometries (ii) the link with WSGGM for non-gray gases–particles mixtures and (iii) incorporation within CFD codes.

Acknowledgments

The financial support for this work was provided by the US Department of Energy (DOE), National Energy Technology Laboratory (NETL), Morgantown, WV, within the Radiation Project for years 2001 and 2002. The work was carried out at Institute for Complex Engineered Systems (ICES), Carnegie Mellon University, Pittsburgh, PA. D.N. Trivic wishes to thank Dr. Thomas J. O'Brien, Research Scientist from DOE, NETL, Morgantown, WV, for having with him many challenging discussions and Cristina H. Amon, Raymond R. Lane Distinguished Professor of Mechanical Engineering, Carnegie Mellon University and Director of ICES for obtaining nice and creative atmosphere in ICES. The hospitality and generosity of lovely people from Carnegie Mellon University and from Pittsburgh must be acknowledged herewith. A part of the support related to the purchasing of an airplane ticket Belgrade-Pittsburgh, of a last generation Dell computer and for final paper writing was provided by Ministry of Science, Technology and Development, Republic of Serbia, within Project No. 1891. Without all these attitudes, activities and financial supports the paper would not be finished and D.N. Trivic would like to express his deep gratitude to all of them.

Appendix A. The equations of Mie theory for spherical particles

A rigorous theory of radiative infrared waves interacting with solid particles, developed for several simple geometries, has been presented by Van de Hulst [21]. The radiation incident on a solid particle is partly absorbed and partly scattered. The scattering is a dispersion of part of the incident radiant energy in different directions. The mathematical description of the interaction between incident radiation and a single solid particle is presented with Maxwell's wave equations. The solution to this problem was obtained by Gustav Mie [21,22], who solved Maxwell's wave equations with the appropriate boundary conditions for single cylindrical and spherical particles. The same problem was solved by Danish physicist Lorenz [23] without using the Maxwell's equations. Lorenz developed his own theory of electromagnetism. Although Lorenz's work predates that of Mie, the general theory related to the scattering of radiation by absorbing spheres is known as "Mie Theory". The basic equations and functions of Mie Theory are summarized below.

The fraction of the energy that is scattered into any given direction, defined by scattering angle γ is given by Scattering Phase Function:

$$\Phi(\gamma) = 2\frac{i_1 + i_2}{x^2 Q_{\text{sca}}} \tag{A.1}$$

The quantities i_1 and i_2 are the non-dimensional polarized intensities, calculated from

$$i_1(x,m,\gamma) = |S_1(\gamma)|^2, \quad i_2(x,m,\gamma) = |S_2(\gamma)|^2 \tag{A.2}$$

The $S_1(\gamma)$ and $S_2(\gamma)$ are the complex amplitude functions, expressed as

$$S_1(\gamma) = \sum_{n=1}^{\infty} \frac{2n+1}{n(n+1)}[a_n \pi_n(\cos\gamma) + b_n \tau_n(\cos\gamma)] \tag{A.3}$$

$$S_2(\gamma) = \sum_{n=1}^{\infty} \frac{2n+1}{n(n+1)}[b_n \pi_n(\cos\gamma) + a_n \tau_n(\cos\gamma)] \tag{A.4}$$

The direction-dependent functions, also called angular functions, π_n and τ_n are related to the Legendre Polynomials $P_n(\cos\gamma)$ as

$$\pi_n(\cos\gamma) = \frac{\mathrm{d}P_n(\cos\gamma)}{\mathrm{d}(\cos\gamma)} \tag{A.5}$$

$$\tau_n(\cos\gamma) = \cos\gamma\,\pi_n(\cos\gamma) - \sin^2\gamma \frac{\mathrm{d}\pi_n(\cos\gamma)}{\mathrm{d}(\cos\gamma)} \tag{A.6}$$

The Mie scattering coefficients a_n and b_n are complex functions of x and z,

$$a_n = \frac{\psi_n'(z)\psi_n(x) - m\psi_n(z)\psi_n'(x)}{\psi_n'(z)\xi_n(x) - m\psi_n(z)\xi_n'(x)} \tag{A.7}$$

$$b_n = \frac{m\psi_n'(z)\psi_n(x) - \psi_n(z)\psi_n'(x)}{m\psi_n'(z)\xi_n(x) - \psi_n(z)\xi_n'(x)} \tag{A.8}$$

where $m = n - \mathrm{i}k$ is complex index of refraction, $x = 2\pi r/\lambda$ is particle size parameter and $z = mx$, and

$$\psi_n'(z) = \frac{\mathrm{d}\psi_n(z)}{\mathrm{d}z} \tag{A.9}$$

$$\xi_n'(x) = \frac{\mathrm{d}\xi_n(z)}{\mathrm{d}z}. \tag{A.10}$$

The functions $\psi_n(z)$ and $\xi_n(x)$ are the Ricatti–Bessel and Ricatti–Hankel functions, respectively. They can be written as

$$\psi_n(z) = z j_n(z) \tag{A.11}$$

$$\xi_n(x) = z j_n(z) - \mathrm{i}z y_n(z) \tag{A.12}$$

where $j_n(z)$ and $y_n(z)$ are spherical Bessel functions of the first and second kinds, respectively.

The efficiency factors for extinction, scattering and absorption, Q_{ext}, Q_{sca} and Q_{abs} are given by

$$Q_{\text{ext}} = \frac{2}{x^2}\sum_{n=1}^{\infty}(2n+1)\mathrm{Re}\{A_n + B_n\} \tag{A.13}$$

$$Q_{\text{sca}} = \frac{2}{x^2}\sum_{n=1}^{\infty}(2n+1)(|A_n|^2 + |B_n|^2) \tag{A.14}$$

where

$$Q_{abs} = Q_{ext} - Q_{sca} \tag{A.15}$$

and

$$A_n = i(-1)^n a_n \tag{A.16}$$

$$B_n = -i(-1)^n b_n \tag{A.17}$$

Computer program developed within this study calculates all of these quantities for spherical particles for given: (i) particle diameter, (ii) complex refractive index of particle material and (iii) value for the wavelength of incident radiation. The evaluation of the infinite series in the relations was terminated, as suggested by Deirmendjian et al. [24], when

$$n = 1.2x + 9 \tag{A.18}$$

References

[1] W.A. Fiveland, Discrete-ordinates solutions of the radiative transport equation for rectangular enclosures, J. Heat Transfer 106 (1984) 699–706.

[2] S.T. Thynell, M.N. Ozisik, Radiation transfer in isotropically scattering rectangular enclosures, J. Thermophys. 1 (1) (1987) 69–76.

[3] A.C. Ratzel III, J.R. Howell, Two-dimensional radiation in absorbing–emitting–scattering media using P–N approximation, ASME Paper 82-HT-19, 1982.

[4] M.P. Menguc, R. Viscanta, Radiative transfer in three-dimensional rectangular enclosures containing inhomogeneous, anisotropically scattering media, J. Quant. Spectrosc. Radiat. Transfer 33 (6) (1985) 533–549.

[5] A.L. Crosbie, R.G. Schrenker, Multiple scattering in two-dimensional rectangular medium exposed to collimated radiation, J. Quant. Spectrosc. Radiat. Transfer 33 (2) (1985) 101–125.

[6] D.N. Trivic, Mathematical modeling of three-dimensional turbulent flow with combustion and radiation, Ph.D. Thesis, Department of Chemical Engineering, University of New Brunswick, Fredericton, N.B., Canada, 1987.

[7] F.R. Steward, D.N. Trivic, An assessment of particle radiation in a pulverized-coal-fired boiler, J. Inst. Energy 452 (1989) 138–146.

[8] T.K. Kim, H. Lee, Effect of anisotropic scattering on radiative heat transfer in two-dimensional enclosures, Int. J. Heat Mass Transfer 31 (8) (1988) 1711–1721.

[9] M.J. Yu, S.W. Beak, J.H. Park, An extension of the weighted sum of gray gases non-gray gas radiation model to a two phase mixture of non-gray gas with particles, Int. J. Heat Mass Transfer 43 (2000) 1699–1713.

[10] T.F. Smith, Z.F. Shen, J.N. Fridman, Evaluation of coefficients for the weighted sum of gray gases model, ASME J. Heat Transfer 104 (1982) 602–608.

[11] M.F. Modest, Radiative Heat Transfer, McGraw Hill Inc., New York, 1993.

[12] V.P. Solovjev, B.W. Webb, An efficient method for modeling radiative transfer in multicomponent gas mixture with soot, Trans. ASME 123 (2001) 450–457.

[13] N.W. Bressloff, The influence of soot loading on weighted-sum-of-gray-gases solutions to the radiative transfer equation across mixtures of gases and soot, Int. J. Heat Mass Transfer 42 (1999) 3469–3480.

[14] M.N. Ozisik, Radiative Transfer, A Wiley-Interscience Publication, Wiley, New York, 1973.

[15] R. Siegel, J.R. Howell, Thermal Radiation Heat Transfer, Hemisphere Publishing Corporation, New York, 1993.

[16] M.F. Modest, Radiative Heat Transfer, Academic Press, New York, 2003.

[17] J.C. Chai, Finite volume method for radiation heat transfer, Ph.D. Dissertation, University of Minnesota, Minneapolis, MN, 1994.

[18] J.C. Chai, H.S. Lee, S.V. Patankar, Finite volume method for radiation heat transfer, J. Thermophys. Heat Transfer 8 (3) (1994) 419–425.

[19] J.C. Chai, S.V. Patankar, in: Minkowitz, Sparrow (Eds.), Finite Volume Method for Radiation Heat Transfer, Advances in Numerical Heat Transfer, vol. 2, Taylor & Francis, 2000.

[20] D.N. Trivic, Modeling of 3-D non-gray gases radiation by coupling the finite volume method with weighted sum of gray gases model, Int. J. Heat Mass Transfer 47 (2004) 1367–1382.

[21] H.C. Van de Hulst, Light Scattering by Small Particles, John Wiley and Sons Inc., 1957.

[22] C.F. Chromey, Evaluation of Mie equations for colored spheres, J. Opt. Soc. Am. 50 (1960) 730.

[23] L. Lorenz, in: Videnscab Selscab Scrifter, vol. 6, Copenhagen, Denmark, 1890.

[24] D. Deirmendjian, R. Clasen, V. Viezee, Mie scattering with complex index of refraction, J. Opt. Soc. Am. 51 (1961) 620.